

Screening two-dimensional materials with topological flat bands

Hang Liu,^{1,2,3} Sheng Meng,^{2,3,*} and Feng Liu^{1,†}

¹*Department of Materials Science and Engineering, University of Utah, Salt Lake City, Utah 84112, USA*

²*Songshan Lake Materials Laboratory, Dongguan, Guangdong 523808, People's Republic of China*

³*Beijing National Laboratory for Condensed Matter Physics and Institute of Physics, Chinese Academy of Sciences, Beijing 100190, People's Republic of China*



(Received 21 April 2021; revised 23 June 2021; accepted 20 July 2021; published 16 August 2021)

The topological flat band (TFB) has been proposed theoretically in various lattice models, to exhibit a rich spectrum of intriguing physical behaviors. However, the experimental demonstration of flat band (FB) properties has been severely hindered by the lack of materials realization. Here, by screening materials from a first-principles materials database, we identify a group of two-dimensional materials with TFBs near the Fermi level, covering some simple line-graph and generalized line-graph FB lattice models. These include the kagome sublattice of O in TiO₂ yielding a spin-unpolarized TFB, and that of V in ferromagnetic V₃F₈ yielding a spin-polarized TFB. The monolayer Nb₃TeCl₇ and its counterparts from element substitution are found to be breathing-kagome-lattice crystals. The family of monolayer III₂VI₃ compounds exhibit a TFB representing the coloring-triangle lattice model. ReF₃, MnF₃, and MnBr₃ are all predicted to be diatomic-kagome-lattice crystals, with TFB transitions induced by atomic substitution. Finally, HgF₂, CdF₂, and ZnF₂ are discovered to host dual TFBs in the diamond-octagon lattice. Our findings pave the way to further experimental exploration of eluding FB materials and properties.

DOI: [10.1103/PhysRevMaterials.5.084203](https://doi.org/10.1103/PhysRevMaterials.5.084203)

Introduction. The destructive interference of wave functions in a crystal lattice gives rise to a type of electronic band without dispersion, dubbed as topological/singular flat bands (TFBs) [1–5]. Without spin-orbit coupling (SOC), the TFB can be identified by the presence of a band touching point with a dispersive band at a high-symmetric k point, where its singular Bloch wave functions in reciprocal space manifest the emergence of topological noncontractible edge states in real space [4,5]; it differs from an isolated trivial flat band (FB) with nonsingular Bloch wave functions, such as the dangling-bond states. With SOC, the degeneracy at the touching point is lifted, leading to the gapped 2D TFB with a nonzero (spin) Chern invariant [4]. The nontrivial topology and the inherently strong electron-electron interaction due to vanishing electron kinetic energy render the TFB a rich spectrum of physical phenomena, such as fractional quantum anomalous Hall effect [6–8], ferromagnetism [9,10], Wigner crystallization [11,12], superconductivity [13], excitonic insulator state [14,15], and excited quantum anomalous/spin Hall effect [16].

Various lattice models have been theoretically proposed to host the TFB. These models are generally based on line-graph construction [17–19], such as the kagome [6,19,20], Lieb [21,22], breathing-kagome [23–26], diatomic-kagome [16,27], coloring-triangle lattices [28], and the diamond-octagon lattice (i.e., line-graph lattice of Lieb lattice) [2,29]. Also, the square and honeycomb lattices,

with multiple atomic orbitals on each lattice site, can host TFBs [3,11,30–32]. On the other hand, however, very few electronic FB materials [33–42] have been identified, either experimentally or computationally, and realizations of the known FB lattice models are rather limited in general, with only a few examples such as the breathing-kagome lattice in Fe₃Sn₂ [41], and the coloring-triangle lattice in Cu-dicyanobenzene monolayer [42] presented so far. This, apparently, has severely hindered the experimental realization of eluding FB properties. It is worth noting that the experimental discovery of FB-associated superconductivity in twisted bilayer graphene [43] has generated a lot of excitement recently, and a surprising ferromagnetic covalent-organic framework without transition-metal atoms [44] has been shown to be originated from a FB [10]. Therefore, computational design and identification of new FB materials, already exist or to be fabricated, is highly desirable to significantly advance the study of TFB physics, materials, and devices.

On the other hand, the recent establishment of materials databases has enabled a high-throughput screening approach to discovering new materials in batches. For example, all the three-dimensional (3D) nonmagnetic topological crystals are screened for compiling a complete catalog of topological materials [45–47]; various nontrivial magnetic crystals are identified from 2D and 3D materials databases [48,49]. Here, by screening the 2D MatPedia database [50] for 2D crystalline materials, we have identified 15 monolayer atomic crystals hosting TFBs near the Fermi level, which cover six different FB lattice models. Among them, the kagome sublattice of O in TiO₂ supports a spin-unpolarized TFB, and that of V in ferromagnetic V₃F₈ supports a spin-polarized TFB. Monolayer

*smeng@iphy.ac.cn

†fliu@eng.utah.edu

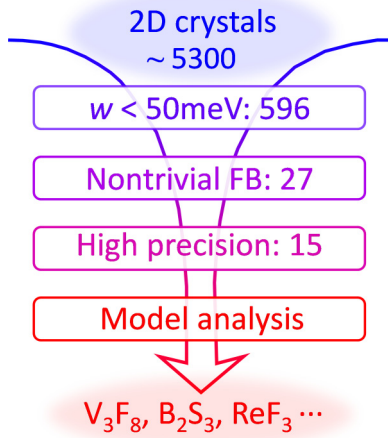


FIG. 1. Flowchart of computational screening for 2D crystals with ideal TFBs.

Nb_3TeCl_7 and its counterparts from element substitution, whose layered 3D structures were already synthesized over two decades ago, are found to be breathing-kagome crystals with possible high-order topology. The family of monolayer III_2VI_3 compounds exhibit a TFB representing the coloring-triangle lattice model. ReF_3 , MnF_3 , and MnBr_3 are all predicted to be diatomic-kagome crystals, with TFB transitions induced by atomic substitution. HgF_2 , CdF_2 , and ZnF_2 are discovered to host dual TFBs in the diamond-octagon lattice. Overall, some existing simple line-graph and generalized line-graph FB lattice models have been identified with several candidate materials.

Screening procedure. Our screening for 2D materials having TFBs starts with the database of 2D MatPedia, which contains electronic band structure without SOC for ~ 5300 monolayer atomic crystals [50], as shown in Fig. 1. The bandwidth w of 11 bands (chosen for FB searching in this work) around the Fermi level is calculated, from which 354 nonmagnetic and 242 magnetic materials are revealed to possess bands whose w is less than 50 meV. We note that the choice of this bandwidth threshold could be somewhat arbitrary, and we used a value that lies in the typical range of the SOC-induced energy gap in realistic solid materials. In general, using a larger (smaller) value one would find more (less) FB materials from screening but a higher (lower) percentage of trivial ones. Next, if the narrow band is identified with a degenerate point with another dispersive band, its host material is selected, amounting to 27 candidate TFB materials [see Tables S1 and S2 in the Supplemental Material (SM) [51]]. Finally, these 27 candidates were further double-checked by *ab initio* calculations with high precision and lattice model analysis (see the computational methods in the SM), which confirmed 15 TFB materials (nine nonmagnetic and six magnetic) representing respectively six different TFB lattice models, as listed in Table I. In the following, we choose the representative examples to show ideal TFBs discovered in (i) kagome lattice, (ii) related breathing-kagome, coloring-triangle, and diatomic-kagome lattices, (iii) diamond-octagon lattice, and (iv) d -orbital graphene lattice.

TABLE I. The discovered monolayer atomic crystals with ideal TFBs.

Model	Nonmagnetic	Magnetic	Space group
Kagome	TiO_2 , BaYSn_4O_7	V_3F_8 , $\text{Li}_2\text{Fe}_3\text{F}_8$	$P-3m1$
Breathing kagome	Nb_3TeCl_7 , Ta_3SBr_7	Nb_3Cl_8	
Coloring triangle	B_2S_3 (III_2VI_3)		$P-62m$
Diatomic kagome	ReF_3	MnF_3 , MnBr_3	$P-3m1$
Honeycomb		VF_3	
Diamond octagon	CdF_2 , ZnF_2 , HgF_2		$P-4m2$

Kagome crystals with the ideal TFB. The well-known kagome lattice consists of three sites in a unit cell, exhibiting two Dirac bands touched with a TFB [Fig. 2(a); see the tight-binding Hamiltonian in the SM]. As shown in Fig. 3(a), the monolayer TiO_2 , a widely studied compound, has O atoms forming an upper and lower kagome layer bridged by O atoms in the middle. It turns out to host a typical kagome band structure from p orbitals of O atoms, with a well separated FB right below the Fermi level while the Dirac bands mix with other trivial bands. As expected, an isolated TFB arises upon a nontrivial gap opening in the presence of SOC [Fig. S1(a) in the SM]. There are also two additional sets of kagome bands far below the Fermi level arising from O $2s$ orbitals in the upper and lower kagome layer, respectively (Fig. S2), sharing a doubly degenerate TFB. Another nonmagnetic kagome crystal is found in monolayer BaYSn_4O_7 , featuring a TFB around the Fermi level arising from Sn atoms sitting on a kagome lattice [Fig. S3(a)]. Previously, kagome bands have been mostly shown in metal-organic and covalent-organic frameworks [35–39]. Here we discover the unknown inorganic 2D materials hosting well-separated kagome bands.

Spin-polarized TFBs are discovered in magnetic kagome crystals with transition-metal elements. As shown in Fig. 3(b), three V atoms in monolayer V_3F_8 (shown to be stable in the literature [55]), with magnetic moment $M = 7 \mu_B$, sit in a kagome sublattice. Naturally, spin-up kagome bands from d orbitals of vanadium atoms arise, with the TFB lying close to the Fermi level based on electron counting. With SOC, a topological gap opens to isolate a Chern TFB [Fig. S1(b)], affording an intriguing possibility of exploring fractional quantum anomalous Hall effect. Another ferromagnetic kagome material is found in monolayer $\text{Li}_2\text{Fe}_3\text{F}_8$, where the kagome sublattice consists of Fe atoms each with $M = 4 \mu_B$ [Fig. S3(b)]. The above-mentioned kagome materials are all intrinsic, without the need of doping, and ideal, without band overlapping with other trivial bands, superior over previous computationally and experimentally identified electronic kagome metals [40, 56–60]. For the kagome materials of TiO_2 and V_3F_8 , their SOC-induced gap opening between the TFB and dispersive bands (Fig. S1) confirms the gapped TFB to possess a nonzero (spin) Chern invariant [4]. Similarly, the TFBs in other identified 2D materials are checked, where the gap is larger for materials with heavier atoms having stronger SOC.

Breathing-kagome crystals with potential second-order topology. When one triangle in a kagome lattice shrinks

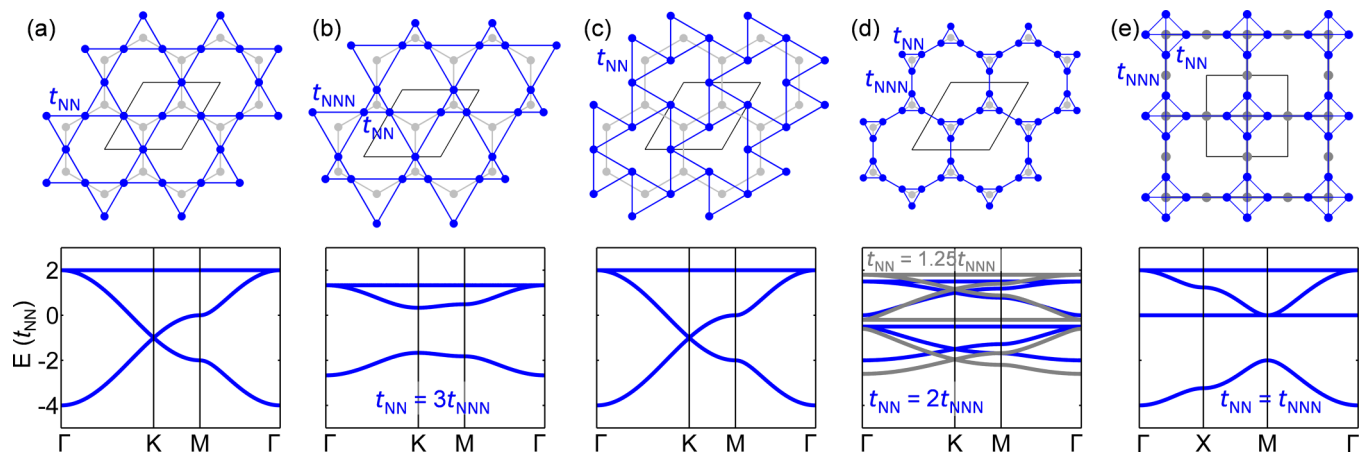


FIG. 2. Lattice structure and tight-binding bands of (a) kagome lattice, and its derivatives including (b) breathing-kagome, (c) coloring-triangle, (d) diatomic-kagome lattices, and (e) diamond-octagon lattice. t_{NN} and t_{NNN} represent the NN and NNN hopping integral, respectively. Gray and blue dots/lines in upper panels show the original lattices and their (generalized) line-graph lattices, respectively. For standard construction, (a) and (e), a line graph takes edge centers of the original graph as its vertices, while for generalized construction, a line graph takes off-edge-center positions, along the edge (b) or off the edge (c), as its vertices. Panel (d) can be viewed as two copies of the generalized line graph in (b), leading to dual FBs.

and the other one expands, a so-called breathing-kagome lattice model is constructed as a generalized line graph of hexagonal lattice [Fig. 2(b)]. This breathing mode does not affect the TFB, but opens a gap at Dirac point to induce

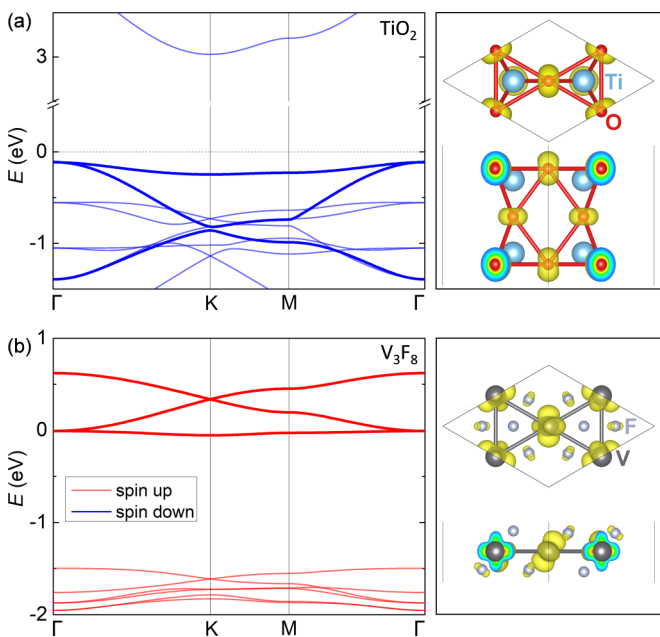


FIG. 3. Ideal kagome bands in monolayer kagome atomic crystals. (a) Oxygen atoms in monolayer TiO_2 form upper and lower kagome layers connected by middle sites, with titanium atoms locating at the center of oxygen tetrahedrons. The electronic structure exhibits obvious kagome bands (bold lines in left panel), and the charge of TFB near the Fermi level is contributed by p orbitals of oxygen atoms (right panel). (b) Vanadium atoms in monolayer V_3F_8 form the perfect kagome lattice, resulting in the typical kagome bands (bold lines in left panel) with a TFB exactly locating at Fermi level. The d orbitals of vanadium atoms contribute to the electron charge of the spin-up kagome bands (right panel).

the second-order topological corner states [23–25,61,62]. As shown in Fig. 4, monolayer Nb_3TeCl_7 is discovered to have Nb atoms locating at the breathing-kagome lattice sites, where Nb d orbitals constitute a clean set of kagome bands with a Dirac gap at the Fermi level. Such a breathing-kagome state is also discovered in 2D Ta_3SBr_7 with Ta atoms locating at the breathing-kagome sites [Fig. S4(a)]. Furthermore, spin-polarized breathing-kagome states with $M = 1 \mu_B$ are discovered in monolayer Nb_3Cl_8 with three Nb atoms sitting at three breathing-kagome sites, respectively [Fig. S4(b)]. While magnetic interaction separates the spin-up and -down bands in energy space, all the features of breathing-kagome bands remain intact. Compared with Nb_3TeCl_7 , the ferromagnetism originates from substituting a Te atom with a Cl atom; compared with V_3F_8 , the breathing deformation in Nb_3Cl_8 originates from substituting V atoms by Nb atoms.

Coloring-triangle crystals with kagome bands. When one triangle in the kagome lattice rotates 30° clockwise and the other triangle 30° counterclockwise, a so-called coloring-triangle lattice, which is another generalized line graph of hexagonal lattice by an off-edge-center construction

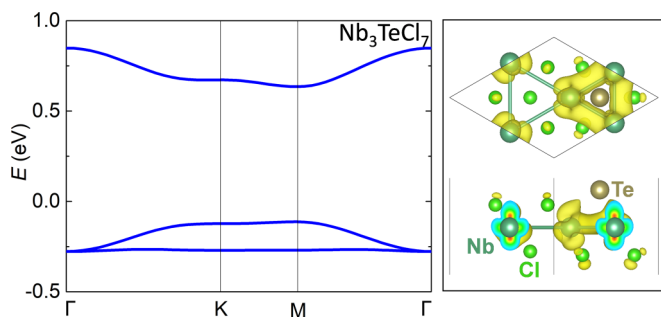


FIG. 4. Left: The electronic structure of monolayer Nb_3TeCl_7 with niobium atoms sitting on a breathing-kagome lattice. Right: Electron charge distribution contributing to the breathing-kagome bands with a gapped Dirac cone in the left.

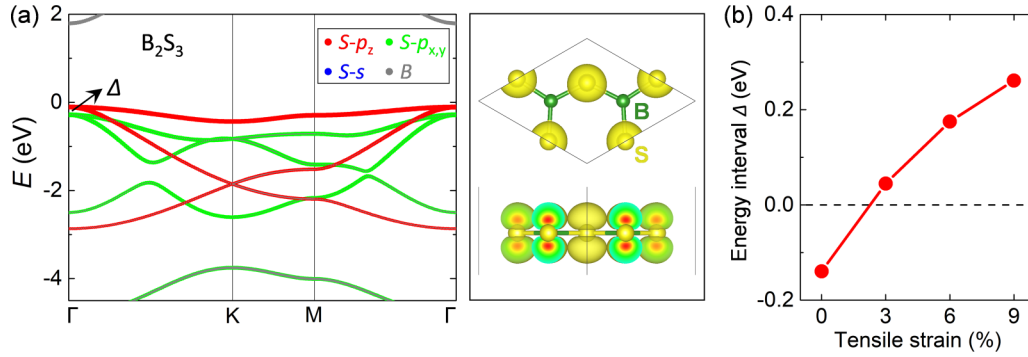


FIG. 5. (a) Electronic structure and orbital composition of monolayer B₂S₃ with +6% tensile strain (left panel). Δ marks the Γ-point energy interval between p_z and $p_{x,y}$ bands just below the Fermi level. The p_z orbitals of sulphur atoms, occupying the sites of a coloring-triangle lattice (right panel), contribute to the TFB of kagome bands near the Fermi level. (b) The variation of Δ with external tensile strain.

[Fig. 2(c)], forms to also host identical kagome bands [28]. The lattice can also be viewed as a triangle lattice with part of nearest-neighbor (NN) hopping being blocked, so that its realization in real crystalline materials is supposed to be quite difficult. Surprisingly, we have overcome this difficulty “accidentally.” As shown in Fig. 5(a), within each unit cell of monolayer B₂S₃, S atoms constitute a triangle sublattice while B atoms are located at the center of two S triangles. Consequently, via the bridging of B atoms, the NN hopping between those S atoms in the two triangles with B are much stronger than those S atoms without bridging B atoms. So, effectively this provides a unique mechanism to selectively block part of NN hopping in a triangle S lattice, as required by the construction of a coloring-triangle lattice. This is clearly confirmed by the perfect kagome bands arising from S p_z orbitals in B₂S₃ [Fig. 5(a)]. The kagome bands are actually embedded in other bands from S $p_{x,y}$ orbitals in the equilibrium B₂S₃ (Fig. S5), but can be separated out by applying a small biaxial tensile strain [Fig. 5(b)], which simultaneously moves the TFB upward closer to the Fermi level. Deep-energy kagome bands from S $3s$ orbitals manifest also the coloring-triangle lattice in monolayer B₂S₃ (Fig. S5).

Similar to B₂S₃, our search reveals that most of the monolayer III₂VI₃ compounds, made from elements in the III and VI main group, exhibit the ideal kagome FBs satisfying the coloring-triangle model upon strain-induced band separation [Table S3, Fig. S6(a)]. An exception is monolayer Tl₂Te₃, for which the kagome states disappear due to the destruction of the desired coloring-triangle hopping, but on the other hand, its strong SOC induces a large topological gap of 0.32 eV [Fig. S6(b)], affording a candidate for high-temperature topological insulator. Also, the FB is absent in monolayer In₂Se₃, Tl₂S₃, and Tl₂Se₃ with large atoms, because of the structure-induced destruction of the desired coloring-triangle hopping (see details in Fig. S7).

TFBs evolution in diatomic-kagome crystals. When every kagome site is replaced by a pair of lattice sites, a diatomic-kagome lattice is formed, which is yet another generalized line graph of hexagonal graph constructed with two copies of breathing-kagome lattices [Fig. 2(d)], leading to intriguing evolution of TFBs and phase transitions [16,27]. For example, with a small next-NN (NNN) hopping integral, two sets of kagome bands coexist [blue lines in

Fig. 2(d)]; as the NNN hopping becomes stronger, the bands evolve into a combination of Dirac bands and $p_{x,y}$ -orbital hexagonal lattice bands [gray lines in Fig. 2(d)], labeled as (D ; $p_{x,y}$) phase [11,30]. Interestingly, our screening process leads to the discovery of three diatomic-kagome crystals, exhibiting the TFB transitions as proposed in tight-binding models. As shown in Fig. 6(a), monolayer ReF₃ has Re atoms sitting on the diatomic-kagome sites, resulting in the (D ; $p_{x,y}$) bands mainly contributed from Re- d orbitals. In contrast, the monolayer MnF₃ and MnBr₃ are ferromagnetic with $M = 4\mu_B$ on each Mn atom, possessing two sets of spin-up kagome and (D ; $p_{x,y}$) bands, respectively [Figs. 6(b) and 6(c)]. From ReF₃ to MnF₃, the (D ; $p_{x,y}$) bands transform into two sets of kagome bands, which in turn transform back into the (D ; $p_{x,y}$) bands from MnF₃ to MnBr₃. This indicates that atomic substitution is an effective way to tune the hopping integrals in diatomic-kagome lattices, providing a promising strategy for topological and FB engineering [63].

Dual TFBs in diamond-octagon crystals. Lieb lattice contains a sublattice of checkerboard lattice which is the line graph of square lattice, and hence possesses FB. The line graph of Lieb lattice (dubbed as diamond-octagon lattice) also possesses FB [2,29]. With four lattice sites in a square unit cell [Fig. 2(e)], when the NN hopping integral is equal to the NNN hopping integral, two perfect TFBs can appear, which are degenerate with one parabolic band in between, with the band touching at Γ and M points, respectively. Due to the usual exponential decay of lattice hopping with distance in real materials, this peculiar model with equal hopping for both closer and farther sites appeared difficult to be realized. Interestingly, in monolayer HgF₂ (Fig. 7), two Hg atoms on the horizontal boundaries of the unit cell are located at different heights from the other two on vertical boundaries. This leads to an almost equal distance between the NN Hg-Hg sites in the same plane to the NNN Hg-Hg sites in the different planes, so as to satisfy the desired electron hopping condition prescribed in the above model [Fig. 2(e)], similar to the case of bilayer Ni(CH) for realizing a diatomic-kagome lattice [16]. Consequently, monolayer HgF₂ exhibits two TFBs inside four bands which are mainly contributed by s orbitals of mercury atoms. Also, this type of dual TFBs is found in monolayer CdF₂ and ZnF₂ (Fig. S8).

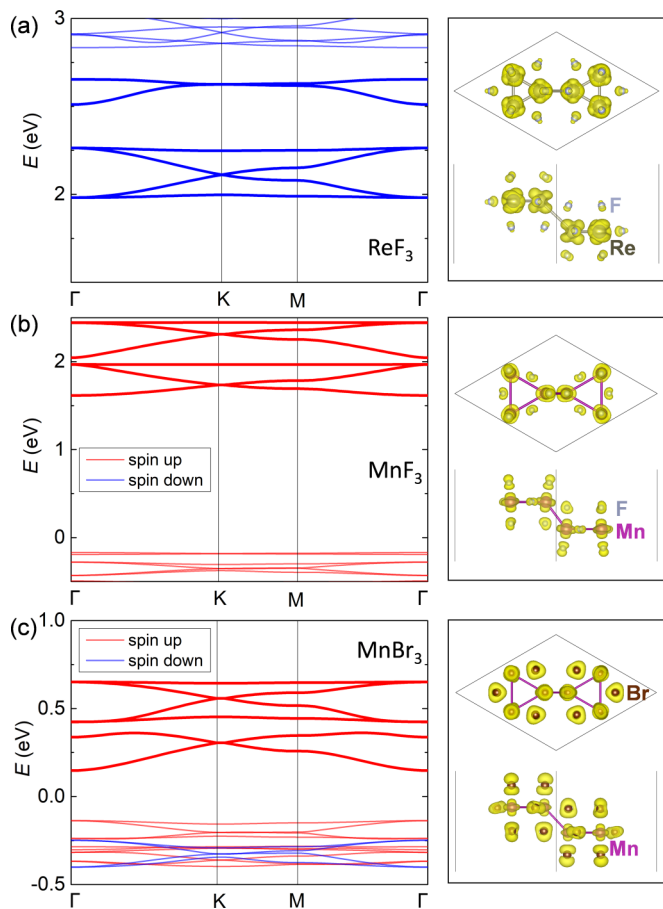


FIG. 6. Atomic and electronic structure for diatomic-kagome crystals of (a) ReF_3 , (b) MnF_3 , and (c) MnBr_3 . Left: Band structure with the diatomic-kagome bands highlighted by thick lines. Right: The distribution of electron charge density for the diatomic-kagome bands highlighted in the left.

Orbital-enabled TFBs in honeycomb crystals. Beyond TFBs from line-graph construction, atomic/molecular orbitals in non-line-graph lattices can also be exploited to produce TFBs [3,11,30–32]. Organometallic framework [11,30,31] and bismuthene on semiconductor substrates [64,65] have been predicted to realize the honeycomb lattice with TFBs

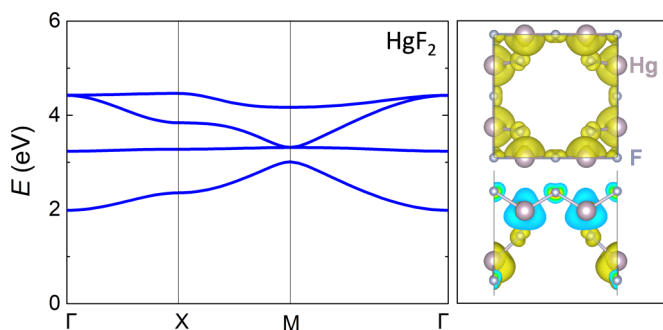


FIG. 7. Dual TFBs in monolayer HgF_2 with a diamond-octagon lattice. Left: Electron band structure. Right: Charge density plot showing the bands in the left are mainly contributed from s orbitals of mercury atoms.

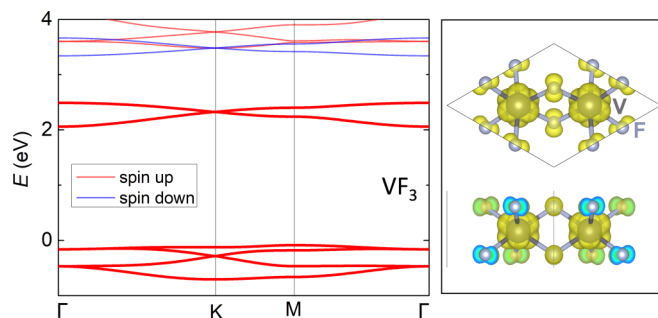


FIG. 8. Honeycomb TFB crystal of monolayer VF_3 . Left: Band structure. Right: Electron charge density distribution contributing to the highlighted bands in the left.

from p orbitals. Here, as shown in Fig. 8, we discover monolayer VF_3 has $V-d$ -orbital TFBs and Dirac bands, which conforms to the recently proposed TFBs from d_{xy} and $d_{x^2-y^2}$ orbitals [3] and Dirac bands from d_{z^2} in a honeycomb lattice, respectively. The TFB is just below the Fermi level and spin polarized, with $M = 2 \mu_B$ on each V atom. In contrast, a previous sd^2 -orbital honeycomb lattice with TFB has been shown in W overlayer on a halogenated Si(111) surface invoking an electronic kagome lattice from the coupled s and d orbitals [32].

In all the above cases, the screening condition for bandwidth $w < 50$ meV is used (Fig. 1). One might relax this condition to discover more FB materials. For example, we also found the monolayer II_1VII_2 compounds, made from elements in the II and VII main groups, have the checkerboard and diamond-octagon FBs with larger bandwidth, where the former arises from an intriguing p -orbital configuration that is equivalent to the diagonal p -orbital orientation in a square lattice [3], such as MgCl_2 shown in Fig. S9 of SM. Totally, two monolayer crystals of VF_3 and MgCl_2 are identified to be non-line-graph materials having the FB near the Fermi level, while others are line-graph FB materials. Beyond the analysis by using tight-binding lattice models, the Wannier construction for FBs of the non-line-graph VF_3 and line-graph V_3F_8 is carried out, which again confirms our finding that they respectively conform to the kagome and honeycomb FB model (see details in Fig. S10).

Potential experimental fabrication and measurement. We note that the 3D layered Nb_3TeCl_7 and Ta_3SBr_7 have been experimentally synthesized over twenty years ago [66,67], making experimental observation of these material-specific breathing-kagome states highly promising. The 2D film of breathing-kagome crystal Nb_3Cl_8 with controllable thickness has been already realized in experiment [68], which calls for immediate experimental confirmation of its predicted TFB. Also, some of the coloring-triangle crystals, such as Ga_2S_3 , are potentially experimentally achievable [69–71]. For other 2D FB crystals predicted here, we expect that they can be exfoliated from layered bulk materials by the mechanical, electrical, or chemical method [72,73], or can be grown on suitable prescreened substrates by the molecular beam epitaxy, or chemical vapor deposition technology [74,75].

The TFBs predicted in this work, all around Fermi level, can be directly probed by angle resolved photoemission

spectroscopy [76], where the momentum-space band dispersion can be measured. Also, the FBs can be probed by scanning tunneling spectroscopy (STS), where a sharp peak of density of states could be shown as a signature for FBs [40], and the edge/corner states from electron topology can be directly imaged by the space-resolved STS. The measurement of quantum Hall conductance can demonstrate topological transport properties [77], which would potentially confirm the intriguing fractional quantum anomalous Hall effect from partially occupied TFBs [6–8].

Conclusions. By employing the data screening calculations on materials from a first-principles materials database, we have discovered 15 inorganic 2D crystals (Table I) with ideal TFBs representing six FB lattice models, which opens a door

towards experimental observation of TFBs in real materials, and exploration/substantiation of their intriguing physics and applications. In particular, some of these realistic 2D crystals have already been made in experiments, which will hopefully draw immediate attention. Moreover, the screening approach developed here for searching 2D FB crystals can be extended to systematically uncovering 3D FB materials from the well-established databases [78–81].

Acknowledgments. F.L. was supported by U.S. DOE-BES (Grant No. DE-FG02-04ER46148). S.M. and H.L. acknowledge financial support from the National Natural Science Foundation of China (Grants No. 12025407 and No. 11934003), and Chinese Academy of Sciences (Grant No. XDB330301).

-
- [1] Z. Liu, F. Liu, and Y.-S. Wu, Exotic electronic states in the world of flat bands: From theory to material, *Chin. Phys. B* **23**, 077308 (2014).
- [2] D.-S. Ma, Y. Xu, C. S. Chiu, N. Regnault, A. A. Houck, Z. Song, and B. A. Bernevig, Spin-Orbit-Induced Topological Flat Bands in Line and Split Graphs of Bipartite Lattices, *Phys. Rev. Lett.* **125**, 266403 (2020).
- [3] H. Liu, G. Sethi, S. Meng, and F. Liu, Orbital design of flat bands in non-line-graph lattices via line-graph wavefunctions, *arXiv:2104.14163*.
- [4] J.-W. Rhim and B.-J. Yang, Classification of flat bands according to the band-crossing singularity of Bloch wave functions, *Phys. Rev. B* **99**, 045107 (2019).
- [5] D. L. Bergman, C. Wu, and L. Balents, Band touching from real-space topology in frustrated hopping models, *Phys. Rev. B* **78**, 125104 (2008).
- [6] E. Tang, J. W. Mei, and X. G. Wen, High-Temperature Fractional Quantum Hall States, *Phys. Rev. Lett.* **106**, 236802 (2011).
- [7] T. Neupert, L. Santos, C. Chamon, and C. Mudry, Fractional Quantum Hall States at Zero Magnetic Field, *Phys. Rev. Lett.* **106**, 236804 (2011).
- [8] K. Sun, Z. Gu, H. Katsura, and S. D. Sarma, Nearly Flatbands with Nontrivial Topology, *Phys. Rev. Lett.* **106**, 236803 (2011).
- [9] E. C. Stoner, Collective electron ferromagnetism, *Proc. R. Soc. London, Ser. A* **165**, 372 (1938).
- [10] W. Jiang, H. Huang, and F. Liu, A Lieb-like lattice in a covalent-organic framework and its Stoner ferromagnetism, *Nat. Commun.* **10**, 2207 (2019).
- [11] C. Wu, D. Bergman, L. Balents, and S. D. Sarma, Flat Bands and Wigner Crystallization in the Honeycomb Optical Lattice, *Phys. Rev. Lett.* **99**, 070401 (2007).
- [12] B. Jaworowski, A. D. Güçlü, P. Kaczmarkiewicz, M. Kupczyński, P. Potasz, and A. Wójs, Wigner crystallization in topological flat bands, *New J. Phys.* **20**, 063023 (2018).
- [13] S. Miyahara, S. Kusuta, and N. Furukawa, BCS theory on a flat band lattice, *Phys. C (Amsterdam, Neth.)* **460**, 1145 (2007).
- [14] D. Jérôme, T. M. Rice, and W. Kohn, Excitonic insulator, *Phys. Rev.* **158**, 462 (1967).
- [15] G. Sethi, Y. Zhou, L. Zhu, L. Yang, and F. Liu, Flat-Bands-Enabled Triplet Excitonic Insulator in a Di-Atomic (Yin-Yang) Kagome Lattice, *Phys. Rev. Lett.* **126**, 196403 (2021).
- [16] Y. Zhou, G. Sethi, H. Liu, Z. Wang, and F. Liu, Excited quantum Hall effect: Enantiomorphic flat bands in a Yin-Yang Kagome lattice, *arXiv:1908.03689*.
- [17] A. Mielke, Ferromagnetic ground states for the Hubbard model on line graphs, *J. Phys. A: Math. Gen.* **24**, L73 (1991).
- [18] A. Mielke, Ferromagnetism in the Hubbard model on line graphs and further considerations, *J. Phys. A: Math. Gen.* **24**, 3311 (1991).
- [19] A. Mielke, Exact ground states for the Hubbard model on the Kagome lattice, *J. Phys. A: Math. Gen.* **25**, 4335 (1992).
- [20] I. Syözi, Statistics of kagomé lattice, *Prog. Theor. Phys.* **6**, 306 (1951).
- [21] E. H. Lieb, Two Theorems on the Hubbard Model, *Phys. Rev. Lett.* **62**, 1201 (1989).
- [22] H. Tasaki, From Nagaoka's ferromagnetism to flat-band ferromagnetism and beyond, *Prog. Theor. Phys.* **99**, 489 (1998).
- [23] M. Ezawa, Higher-Order Topological Insulators and Semimetals on the Breathing Kagome and Pyrochlore Lattices, *Phys. Rev. Lett.* **120**, 026801 (2018).
- [24] H. Xue, Y. Yang, F. Gao, Y. Chong, and B. Zhang, Acoustic higher-order topological insulator on a kagome lattice, *Nat. Mater.* **18**, 108 (2019).
- [25] A. Bolens and N. Nagaosa, Topological states on the breathing kagome lattice, *Phys. Rev. B* **99**, 165141 (2019).
- [26] K. Essafi, L. D. C. Jaubert, and M. Udagawa, Flat bands and Dirac cones in breathing lattices, *J. Phys.: Condens. Matter* **29**, 315802 (2017).
- [27] Y. Zhou, G. Sethi, C. Zhang, X. Ni, and F. Liu, Giant intrinsic circular dichroism of enantiomorphic flat Chern bands and flatband devices, *Phys. Rev. B* **102**, 125115 (2020).
- [28] S. Zhang, M. Kang, H. Huang, W. Jiang, X. Ni, L. Kang, S. Zhang, H. Xu, Z. Liu, and F. Liu, Kagome bands disguised in a coloring-triangle lattice, *Phys. Rev. B* **99**, 100404(R) (2019).
- [29] B. Pal, Nontrivial topological flat bands in a diamond-octagon lattice geometry, *Phys. Rev. B* **98**, 245116 (2018).
- [30] C. Wu and S. D. Sarma, $p_{x,y}$ -orbital counterpart of graphene: Cold atoms in the honeycomb optical lattice, *Phys. Rev. B* **77**, 235107 (2008).
- [31] Z. Liu, Z. F. Wang, J. W. Mei, Y. S. Wu, and F. Liu, Flat Chern Band in a Two-Dimensional Organometallic Framework, *Phys. Rev. Lett.* **110**, 106804 (2013).

- [32] M. Zhou, Z. Liu, W. Ming, Z. Wang, and F. Liu, *sd² Graphene: Kagome Band in a Hexagonal Lattice*, *Phys. Rev. Lett.* **113**, 236802 (2014).
- [33] X. Zhang and M. Zhao, Robust half-metallicity and topological aspects in two-dimensional Cu-TPyB, *Sci. Rep.* **5**, 14098 (2015).
- [34] O. J. Silveira, S. S. Alexandre, and H. Chacham, Electron states of 2D metal-organic and covalent-organic honeycomb frameworks: Ab initio results and a general fitting hamiltonian, *J. Phys. Chem. C* **120**, 19796 (2016).
- [35] Z. F. Wang, N. Su, and F. Liu, Prediction of a two-dimensional organic topological insulator, *Nano Lett.* **13**, 2842 (2013).
- [36] M. G. Yamada, T. Soejima, N. Tsuji, D. Hirai, M. Dincă, and H. Aoki, First-principles design of a half-filled flat band of the kagome lattice in two-dimensional metal-organic frameworks, *Phys. Rev. B* **94**, 081102(R) (2016).
- [37] L. Z. Zhang, Z. F. Wang, B. Huang, B. Cui, Z. Wang, S. X. Du, H. J. Gao, and F. Liu, Intrinsic Two-Dimensional Organic Topological Insulators in Metal-Dicyanoanthracene Lattices, *Nano Lett.* **16**, 2072 (2016).
- [38] X. Zhang, Z. Wang, M. Zhao, and F. Liu, Tunable topological states in electron-doped HTT-Pt, *Phys. Rev. B* **93**, 165401 (2016).
- [39] O. J. Silveira and H. Chacham, Electronic and spin-orbit properties of the kagome MOF family $M_3(1, 2, 5, 6, 9, 10 - \text{triphenylenehexathiol})_2$ ($M = \text{Ni, Pt, Cu}$ and Au), *J. Phys.: Condens. Matter* **29**, 09LT01 (2017).
- [40] Z. Li, J. Zhuang, L. Wang, H. Feng, Q. Gao, X. Xu, W. Hao, X. Wang, C. Zhang, K. Wu, S. X. Dou, L. Chen, Z. Hu, and Y. Du, Realization of flat band with possible nontrivial topology in electronic Kagome lattice, *Sci. Adv.* **4**, eaau4511 (2018).
- [41] H. Tanaka, Y. Fujisawa, K. Kuroda, R. Noguchi, S. Sakuragi, C. Bareille, B. Smith, C. Cacho, S. W. Jung, T. Muro, Y. Okada, and T. Kondo, Three-dimensional electronic structure in ferromagnetic Fe_3Sn_2 with breathing kagome bilayers, *Phys. Rev. B* **101**, 161114(R) (2020).
- [42] Y. Gao, Y.-Y. Zhang, J.-T. Sun, L. Zhang, S. Zhang, and S. Du, Quantum anomalous Hall effect in two-dimensional Cucyanobenzene coloring-triangle lattice, *Nano Res.* **13**, 1571 (2020).
- [43] Y. Cao, V. Fatemi, S. Fang, K. Watanabe, T. Taniguchi, E. Kaxiras, and P. Jarillo-Herrero, Unconventional superconductivity in magic-angle graphene superlattices, *Nature (London)* **556**, 43 (2018).
- [44] E. Jin, M. Asada, Q. Xu, S. Dalapati, M. A. Addicoat, M. A. Brady, H. Xu, T. Nakamura, T. Heine, Q. Chen, and D. Jiang, Two-dimensional sp^2 carbon-conjugated covalent organic frameworks, *Science* **357**, 673 (2017).
- [45] F. Tang, H. C. Po, A. Vishwanath, and X. Wan, Comprehensive search for topological materials using symmetry indicators, *Nature (London)* **566**, 486 (2019).
- [46] M. G. Vergniory, L. Elcoro, C. Felser, N. Regnault, B. A. Bernevig, and Z. Wang, A complete catalogue of high-quality topological materials, *Nature (London)* **566**, 480 (2019).
- [47] T. Zhang, Y. Jiang, Z. Song, H. Huang, Y. He, Z. Fang, H. Weng, and C. Fang, Catalogue of topological electronic materials, *Nature (London)* **566**, 475 (2019).
- [48] H. Liu, J. T. Sun, M. Liu, and S. Meng, Screening magnetic two-dimensional atomic crystals with nontrivial electronic topology, *J. Phys. Chem. Lett.* **9**, 6709 (2018).
- [49] Y. Xu, L. Elcoro, Z.-D. Song, B. J. Wieder, M. G. Vergniory, N. Regnault, Y. Chen, C. Felser, and B. A. Bernevig, High-throughput calculations of magnetic topological materials, *Nature (London)* **586**, 702 (2020).
- [50] J. Zhou, L. Shen, M. D. Costa, K. A. Persson, S. P. Ong, P. Huck, Y. Lu, X. Ma, Y. Chen, H. Tang, and Y. P. Feng, 2DMat-Pedia, an open computational database of two-dimensional materials from top-down and bottom-up approaches, *Sci. Data* **6**, 86 (2019).
- [51] See Supplemental Material at <http://link.aps.org/supplemental/10.1103/PhysRevMaterials.5.084203> for details about computational methods, list of TFB materials, SOC bands, tight-binding modeling, and bands of TFB materials not shown in main text, which includes Refs. [3,52–54].
- [52] G. Kresse and J. Furthmüller, Efficient iterative schemes for ab initio total-energy calculations using a plane-wave basis set, *Phys. Rev. B* **54**, 11169 (1996).
- [53] J. P. Perdew, K. Burke, and M. Ernzerhof, Generalized Gradient Approximation Made Simple, *Phys. Rev. Lett.* **77**, 3865 (1996).
- [54] A. A. Mostofi, J. R. Yates, G. Pizzi, Y.-S. Lee, I. Souza, D. Vanderbilt, and N. Marzari, An updated version of wannier90: A tool for obtaining maximally-localised Wannier functions, *Comput. Phys. Commun.* **185**, 2309 (2014).
- [55] H. Xiao, X. Wang, R. Wang, L. Xu, S. Liang, and C. Yang, Intrinsic magnetism and biaxial strain tuning in two-dimensional metal halides V_3X_8 ($X = \text{F, Cl, Br, I}$) from first principles and Monte Carlo simulation, *Phys. Chem. Chem. Phys.* **21**, 11731 (2019).
- [56] M. Kang, S. Fang, L. Ye, H. C. Po, J. Denlinger, C. Jozwiak, A. Bostwick, E. Rotenberg, E. Kaxiras, J. G. Checkelsky, and R. Comin, Topological flat bands in frustrated kagome lattice CoSn , *Nat. Commun.* **11**, 4004 (2020).
- [57] B. R. Ortiz, S. M. L. Teicher, Y. Hu, J. L. Zuo, P. M. Sarte, E. C. Schueller, A. M. M. Abeykoon, M. J. Krogstad, S. Rosenkranz, R. Osborn, R. Seshadri, L. Balents, J. He, and S. D. Wilson, CsV_3Sb_5 : A \mathbb{Z}_2 Topological Kagome Metal with a Superconducting Ground State, *Phys. Rev. Lett.* **125**, 247002 (2020).
- [58] L. Ye, M. Kang, J. Liu, F. von Cube, C. R. Wicker, T. Suzuki, C. Jozwiak, A. Bostwick, E. Rotenberg, D. C. Bell, L. Fu, R. Comin, and J. G. Checkelsky, Massive Dirac fermions in a ferromagnetic kagome metal, *Nature (London)* **555**, 638 (2018).
- [59] Z. Lin, J. H. Choi, Q. Zhang, W. Qin, S. Yi, P. Wang, L. Li, Y. Wang, H. Zhang, Z. Sun, L. Wei, S. Zhang, T. Guo, Q. Lu, J. H. Cho, C. Zeng, and Z. Zhang, Flatbands and Emergent Ferromagnetic Ordering in Fe_3Sn_2 Kagome Lattices, *Phys. Rev. Lett.* **121**, 096401 (2018).
- [60] M. Kang, L. Ye, S. Fang, J. S. You, A. Levitan, M. Han, J. I. Facio, C. Jozwiak, A. Bostwick, E. Rotenberg, M. K. Chan, R. D. McDonald, D. Graf, K. Kaznatcheev, E. Vescovo, D. C. Bell, E. Kaxiras, J. van den Brink, M. Richter, M. Prasad Ghimire, J. G. Checkelsky, and R. Comin, Dirac fermions and flat bands in the ideal kagome metal FeSn , *Nat. Mater.* **19**, 163 (2020).
- [61] X. Ni, M. Weiner, A. Alu, and A. B. Khanikaev, Observation of higher-order topological acoustic states protected by generalized chiral symmetry, *Nat. Mater.* **18**, 113 (2019).
- [62] S. N. Kempkes, M. R. Slot, J. J. van den Broeke, P. Capiod, W. A. Benalcazar, D. Vanmaekelbergh, D. Bercioux, I. Swart, and C. M. Smith, Robust zero-energy modes in an electronic higher-order topological insulator, *Nat. Mater.* **18**, 1292 (2019).

- [63] B. Huang, M. Yoon, B. G. Sumpter, S. H. Wei, and F. Liu, Alloy Engineering of Defect Properties in Semiconductors: Suppression of Deep Levels in Transition-Metal Dichalcogenides, *Phys. Rev. Lett.* **115**, 126806 (2015).
- [64] M. Zhou, W. Ming, Z. Liu, Z. Wang, P. Li, and F. Liu, Epitaxial growth of large-gap quantum spin Hall insulator on semiconductor surface, *Proc. Natl. Acad. Sci. USA* **111**, 14378 (2014).
- [65] M. Zhou, W. Ming, Z. Liu, Z. Wang, Y. Yao, and F. Liu, Formation of quantum spin Hall state on Si surface and energy gap scaling with strength of spin orbit coupling, *Sci. Rep.* **4**, 7102 (2014).
- [66] G. J. Miller, Solid state chemistry of Nb_3Cl_8 : Nb_3TeCl_7 , mixed crystal formation, and intercalation, *J. Alloys Compd.* **217**, 5 (1995).
- [67] M. Smith and G. J. Miller, Ta_3SBr_7 — A new structure type in the M_3QX_7 family ($M = \text{Nb, Ta}$; $Q = \text{S, Se, Te}$; $X = \text{Cl, Br, I}$), *J. Solid State Chem.* **140**, 226 (1998).
- [68] J. Yoon, E. Lesne, K. Sklarek, J. Sheckelton, C. Pasco, S. S. P. Parkin, T. M. McQueen, and M. N. Ali, Anomalous thickness-dependent electrical conductivity in van der Waals layered transition metal halide, Nb_3Cl_8 , *J. Phys.: Condens. Matter* **32**, 304004 (2020).
- [69] M. M. Y. A. Alsaif, N. Pillai, S. Kuriakose, S. Walia, A. Jannat, K. Xu, T. Alkathiri, M. Mohiuddin, T. Daeneke, K. Kalantar-Zadeh, J. Z. Ou, and A. Zavabeti, Atomically thin Ga_2S_3 from skin of liquid metals for electrical, optical, and sensing applications, *ACS Appl. Nano Mater.* **2**, 4665 (2019).
- [70] X. Wang, Y. Sheng, R. J. Chang, J. K. Lee, Y. Zhou, S. Li, T. Chen, H. Huang, B. F. Porter, H. Bhaskaran, and J. H. Warner, Chemical vapor deposition growth of two-dimensional monolayer gallium sulfide crystals using hydrogen reduction of Ga_2S_3 , *ACS Omega* **3**, 7897 (2018).
- [71] L. Hu and X. Huang, Peculiar electronic, strong in-plane and out-of-plane second harmonic generation and piezoelectric properties of atom-thick $\alpha\text{-M}_2\text{X}_3$ ($M = \text{Ga, In}$; $X = \text{S, Se}$): Role of spontaneous electric dipole orientations, *RSC Adv.* **7**, 55034 (2017).
- [72] K. S. Novoselov, A. Mishchenko, A. Carvalho, and A. H. Castro Neto, 2D materials and van der Waals heterostructures, *Science* **353**, aac9439 (2016).
- [73] K. S. Novoselov, A. K. Geim, S. V. Morozov, D. Jiang, Y. Zhang, S. V. Dubonos, I. V. Grigorieva, and A. A. Firsov, Electric field effect in atomically thin carbon films, *Science* **306**, 666 (2004).
- [74] J. Deng, B. Xia, X. Ma, H. Chen, H. Shan, X. Zhai, B. Li, A. Zhao, Y. Xu, W. Duan, S. C. Zhang, B. Wang, and J. G. Hou, Epitaxial growth of ultraflat stanene with topological band inversion, *Nat. Mater.* **17**, 1081 (2018).
- [75] J. Zhou, J. Lin, X. Huang, Y. Zhou, Y. Chen, J. Xia, H. Wang, Y. Xie, H. Yu, J. Lei, D. Wu, F. Liu, Q. Fu, Q. Zeng, C. H. Hsu, C. Yang, L. Lu, T. Yu, Z. Shen, H. Lin, B. I. Yakobson, Q. Liu, K. Suenaga, G. Liu, and Z. Liu, A library of atomically thin metal chalcogenides, *Nature (London)* **556**, 355 (2018).
- [76] J. Kim, S. S. Baik, S. H. Ryu, Y. Sohn, S. Park, B. G. Park, J. Denlinger, Y. Yi, H. J. Choi, and K. S. Kim, Observation of tunable band gap and anisotropic Dirac semimetal state in black phosphorus, *Science* **349**, 723 (2015).
- [77] C.-Z. Chang, J. Zhang, X. Feng, J. Shen, Z. Zhang, M. Guo, K. Li, Y. Ou, P. Wei, L.-L. Wang, Z.-Q. Ji, Y. Feng, S. Ji, X. Chen, J. Jia, X. Dai, Z. Fang, S.-C. Zhang, K. He, Y. Wang, L. Lu, X.-C. Ma, and Q.-K. Xue, Experimental observation of the quantum anomalous hall effect in a magnetic topological insulator, *Science* **340**, 167 (2013).
- [78] A. Jain, S. P. Ong, G. Hautier, W. Chen, W. D. Richards, S. Dacek, S. Cholia, D. Gunter, D. Skinner, G. Ceder, and K. A. Persson, Commentary: The Materials Project: A materials genome approach to accelerating materials innovation, *APL Mater.* **1**, 011002 (2013).
- [79] S. Curtarolo, W. Setyawan, G. L. W. Hart, M. Jahnatek, R. V. Chepulskii, R. H. Taylor, S. Wang, J. Xue, K. Yang, O. Levy, M. J. Mehl, H. T. Stokes, D. O. Demchenko, and D. Morgan, AFLOW: An automatic framework for high-throughput materials discovery, *Comput. Mater. Sci.* **58**, 218 (2012).
- [80] C. Draxl and M. Scheffler, NOMAD: The FAIR concept for big data-driven materials science, *MRS Bull.* **43**, 676 (2018).
- [81] G. Pizzi, A. Cepellotti, R. Sabatini, N. Marzari, and B. Kozinsky, AiiDA: Automated interactive infrastructure and database for computational science, *Comput. Mater. Sci.* **111**, 218 (2016).